

Article

# Optimization of Buildings Energy Consumption by Designing Sliding Mode Control for Multizone VAV Air Conditioning Systems

Awais Shah <sup>1</sup>, Deqing Huang <sup>1,\*</sup> , Tianpeng Huang <sup>1</sup> and Umar Farid <sup>2</sup> 

<sup>1</sup> School of Electrical Engineering, Southwest Jiaotong University, Chengdu 610031, China; awaishah@my.swjtu.edu.cn (A.S.); tphuang@my.swjtu.edu.cn (T.H.)

<sup>2</sup> Department of Electrical Engineering, Comsats Institute of Information and Technology, Abbottabad 22010, Pakistan; umarfarid@ciit.net.pk

\* Correspondence: elehd@home.swjtu.edu.cn

Received: 26 September 2018; Accepted: 23 October 2018; Published: 25 October 2018

**Abstract:** Variable air volume (VAV) is the most common installation among heating ventilating and air conditioning (HVAC) systems. To maintain the comfort level and lessen energy utilization, there is a pressing need for its effective control. In this study, a lumped parameter model composed of multizone VAV is considered, and sliding mode control (SMC) is designed to guarantee robust operation in the presence of uncertainties. For comparison of the proposed controller performance, a proportional integral derivative (PID) controller is additionally designed. The indoor temperature of zones is controlled by positioning the supply air dampers. Tracking objectives of controllers are inspected via two practical cases of desired temperature setpoints including (a) sinusoidal waveform and (b) the combination of steps. Results obtained using SMC ensure the robust operation of the VAV system against parametric uncertainties. In addition, SMC is more energy efficient than PID in terms of overshoot and settling time.

**Keywords:** variable air volume; sliding mode control; heating ventilation and air conditioning (HVAC); multiple input multiple output (MIMO)

---

## 1. Introduction

Social expectations for the betterment of life standards lead to widespread use of air conditioners in buildings to improve the comfort level for occupants. Indoor air quality (IAQ) is becoming more vital in light of the fact that individuals spend more time inside buildings. On the other hand, there is trade off between the thermal comfort level of occupants and energy consumption. Around 40% of building energy is devoured by heating ventilation and air conditioning (HVAC) systems [1]. The HVAC system utilizes a broad assortment of air conditioning systems. Among those, to achieve thermal comfort for occupants, a variable air volume (VAV) air conditioning system is considered with more energy efficiency [2]. Researchers have carried out a large number of research works to reduce the energy consumption of HVAC while maintaining IAQ and comfort level.

In this paper, we analyzed the aforementioned problem for the specific scenario of VAV. A lumped parameter type model of multizone VAV is considered, and two control strategies, namely (a) sliding mode control (SMC) and (b) proportional integral derivative (PID) control, are designed. The inside temperature of zones is controlled by varying air flow via damper positions. The chilled mass water flow rate in the cooling coil is varied, and duct pressure is kept constant during the operation cycle. By using the VAV system, we can achieve good comfort levels and less energy consumption [3]. In VAV air conditioning systems, the provided air is maintained at a fix temperature, and inside room temperatures are managed by manipulating the volume of air furnished to individual room. The return

air and supply air are regulated in order to maintain static pressure in the duct. The static pressure in the duct is also controlled by varying fan speed in the air handling unit (AHU) [4–6].

The advancement of precise and basic dynamic models for the VAV system is the most vital factor for proficient design. Dynamic models might be changed in structure (straightforward or complex), contingent upon the sort of energy administration capacities and the precision. However, from the functional perspective, inferring straightforward and exact models is of extraordinary significance. Robust sliding mode control (SMC) to increase energy efficiency for the air handling unit (AHU) was designed in [7]. Indoor humidity and temperature were controlled by variation of air by fan speed and refrigerant velocity in the cooling coil. Indoor temperature and humidity dynamic response were modeled via state space modeling in [8]. A two-zone model was presented to observe the dynamic behavior of the indoor environment. The ordinary differential equations representing the thermal behavior of zones were transformed into state space format by linear approximation. The authors in [9] discussed a variable refrigerant flow (VRF) and VAV air conditioning combined control system approach. For this type of combined system, an online optimal control is presented. The results show that the suggested system consumes less energy. However, the hardware complexity due to the hybrid system makes maintenance a difficult task in the long run. An adaptive controller is designed for the decoupled HVAC system via the identification tool box in the system for the control system parameters' enhancement [10]. In [11], the author developed feedback linearization control for VAV air conditioning systems.

An approach to address the baseline performance of the VAV system by characterizing the variations occurring in it was presented in [12], where those variations in the system were identified and classified into different categories. The authors in [13] presented a comprehensive review of two types of control strategies for temperature and humidity control. Firstly, a hardware change like additional dehumidifying in the current HVAC system was suggested. Secondly, simultaneous control of the temperature and humidity control algorithms was studied. In [14], the authors presented and investigative work for multizone buildings in VAV static pressure control by statistically informed data. A control technique to lower the air flow rate in the VAV terminal unit for an office building was presented in [15]. Minimum air was supplied to the terminal unit by keeping IAQ at an acceptable level. Modeling of an augmented HVAC system including CO<sub>2</sub> concentration and its control strategies were presented in [16]. The proposed augmented HVAC system was MIMO and had no relative degree problem; therefore, the dynamic extension algorithm can be employed, then a feedback linearization technique applied. A linear-quadratic regulator (LQR) was designed to optimize control performance and to stabilize the proposed HVAC system.

In [17], VAV optimized control was presented, which utilized ventilation based on average time. The proposed strategy replaced the position of the VAV damper between fully closed and partially open when no cooling was required in a zone. The authors in [18] presented a stepless variable speed drive that was applied in the chiller unit and fan coil of the VAV system. The results of the proposed study show a significant amount of decrease in energy consumption (4.5582 kWh to 2.888 kWh) by using a brushless direct current (DC) motor. At least four different types of strategies to control the VAV system were discussed in [19]. Control Method 'A' used constant air intake and consumed more energy, but had a good comfort level; 'B' reduced energy consumption to 15%; 'C' produced up to 20% energy savings results; outdoor air flow combined with indoor temperature reset can achieve 10% of energy savings, named as Method 'D'. Elman neural networks were used to predict the indoor air temperature of the VAV system in [20]. The basic laws based on the pressure independent and pressure-dependent terminal unit of VAV were designed, then the Elman neural network with control was proposed. The authors in [21] presented models of an air conditioning system, the fundamental components of which were a cooling tower, a water-water chiller and a reference building. The model of the cooling tower was validated by using exploratory information in a pilot plant. The principle objective was to execute an upgrading control methodology with a specific end goal to diminish both energy and water utilization.

Model predictive control (MPC) is also a popular technique used in VAV air conditioning systems. In [22], the authors presented a typical word reference and scientific categorization that gave a shared classification to all the building disciplines engaged with building plan and control. Besides, the principle extent of this paper was to characterize the MPC, detailing the structure and basically discussing the results of various existing MPC calculations for building and HVAC framework administration. The authors in [23] discussed an MPC-based nonlinear control of an air conditioning system for an office in building. Heating and cooling were simultaneously controlled in the office building. The gain linearity and bi-linearity concerned system based on MPC was presented in [24]. Two main processes were discussed in this study, the bi-linearity of the input and output with uncertainty, as well as the gain nonlinearity of the damper system. In [25], MPC was developed to reduce energy consumption by a multizone VAV air handling unit. In [26], the authors exhibited an economic model-based MPC whose fundamental quality was the utilization of the day-ahead value (DAP) to anticipate the energy consumption related to the HVAC.

Health monitoring using a fuzzy neural network for the HVAC system was studied in [27]. Fuzzy logic combined with neural networks was used for a health monitoring system (HMS) in the VAV unit to identify faulty operation of the system. The artificial neural network (ANN) technique was used to distinguish the type of faults in the system. Zijian and Qing in [28] presented an event-based strategy for multiple rooms for an HVAC system for energy saving. The authors in [29] presented a study to examine the distinctive control techniques for HVAC frameworks. The favorable circumstances and detriments of each control technique were talked about, and lastly, the fuzzy cognitive map (FCM) technique was presented as another procedure for HVAC frameworks.

Despite numerous examinations having been performed for dynamic modeling and control of VAV systems, its nonlinear dynamic investigation has not been considered in the past studies. With the existence of nonlinear sources and the multivariable model of VAV, where extraordinary parameters are associated with a complex relation, linear analysis fails to anticipate the phenomena. Furthermore, without a broad pre-learning of VAV system behavior against conceivable uncertainties, the application of the designed controllers may increase energy utilization with a disruptive variable response. Since the HVAC system is uncertainty based and highly nonlinear, SMC may potentially be the best choice because of its insensitive behavior towards disturbances and uncertainties.

The contribution of this paper is that a lumped parameter type nonlinear model of a VAV air conditioning system is examined within the sight of practical harmonic unsettling influences in dynamic state variables. Since the dynamic model of the VAV system is nonlinear, two control techniques, namely (a) sliding mode control and (b) PID control, are developed. The aim is to build accurate and efficient models that can save energy. The temperature setpoint for each zone is achieved by manipulating the position of the supply air damper. The chilled water flow rate in the cooling coil is used to control the temperature of supply air. Two desired commands including a sinusoidal wave form and the sequence of steps are used as a setpoint to ensure robust tracking by the controller. Both models were developed with MATLAB codes, and comparisons will be made on the basis of performance deviations from setpoints and the response to changes in the systems. Furthermore, the setpoint of Zone 1 is different from that of Zone 2, which shows no dynamic coupling loop effect between the zones' supply air temperature.

The system description of the VAV system and its mathematical modeling are described in Section 2. Control laws are adopted in Section 3, and results are presented in Section 4. Finally, the conclusion is drawn in Section 5.

## 2. VAV System Description

The VAV system shown in Figure 1 is a single duct and consists of two thermal zones. Temperature, pressure and air flow sensors are placed at various positions; whereas, VAV boxes, cooling coil, return ducts and fan supply are the main components of system. The system is chosen to be operated in cooling mode. The operational sequence of the system follows as only 25% of fresh air is taken to

mix with recirculated air. After entering the cooling or heating coil, the air is conditioned and then supplied to VAV boxes via the supply air fan monitored by the controller. The VAV boxes supply the air to the rooms according to the temperature setpoints. The return air is collected by the return duct fan, and 25% of its portion is exhausted outdoors by dampers. By assuming constant duct pressure and temperature, the VAV system works in the following way.

- The temperatures of both zones are supervised by the VAV system controller. If the temperature is high, the controller operates the damper position to open, and if the temperature is low, the damper is adjusted to the close position.
- In the case of a fully-occupied zone, the damper cannot be shut down fully and has to maintain fresh air supply at a minimum level (30% of the peak supply volume).

To design controller for the VAV system with the three main loops is given in Table 1.

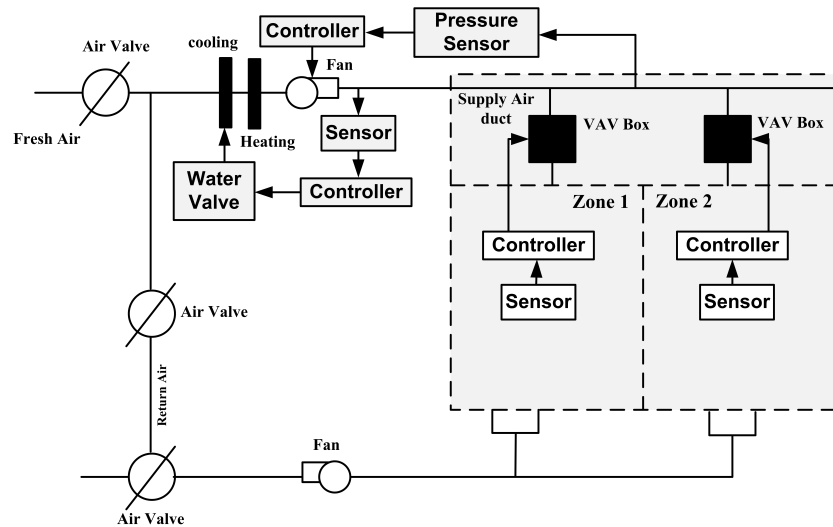


**Figure 1.** System description of the two-zone variable air volume (VAV) system.

**Table 1.** The three control loops of the variable air volume (VAV) air conditioning system.

No.	Controlled Variable	Manipulated Variable
1	Temperature of air supply	Flow rate of water in cooling coil
2	Zone 1 temperature	Air supply to Zone 1 by damper position
3	Zone 2 temperature	Air supply to Zone 2 by damper position

## 2.1. Mathematical Modeling of the VAV System

### 2.1.1. Cooling Coil

The cooling coil works on the principle of a water to air heat exchanger and provides conditioned air. The cooling coil heat transfer equation explains the amount of heat transferred to warm air from the chilled water. The following assumptions are made during the conditioning process of air.

- The properties of the refrigerant do not depend on the variations in temperature for the operating range.
- The inlet temperature of air is the same as the inside air temperature in the coil.
- The heat transfer to air from the coil mass is steady.

The heat dynamics of the cooling coil are described by the following relation.

$$\begin{aligned}
 M_{cc}H_{cc}\dot{T}_{cc} &= \dot{m}_{cw}H_{cw}(T_{cwi} - T_{cwo}) + \tau_a(T_{sai} - T_{cc}) \\
 \dot{m}_{sa}H_{sa}(T_{sao} - T_{sai}) &= \tau_a(T_{cc} - T_{sai}),
 \end{aligned}
 \tag{1}$$

where  $M_{cc}$ ,  $H_{cc}$  and  $T_{cc}$  are the cooling coil mass, cooling coil heat capacity and cooling coil temperature.  $\dot{m}_{cw}$ ,  $H_{cw}$ ,  $T_{cwi}$ ,  $T_{cwo}$ ,  $\tau_a$  and  $T_{sai}$  are the mass flow rate of cold water, cold water heat capacity, cooling coil inlet water temperature, cooling coil outlet water temperature, the coefficient of heat exchange and supply air inlet temperature to the coil, respectively.  $\dot{m}_{sa}$ ,  $H_{sa}$  and  $T_{sao}$  are the supply air flow rate, supply air heat capacity and supply air outlet temperature to the coil. In Equation (1),

$$\begin{aligned} \dot{T}_{sao} &= \left[ \frac{\dot{m}_{cw} H_{cw} (T_{cwi} - T_{cwo}) + (T_{sai} - T_{sao})}{\dot{m}_{sa} H_{sa}} \right] \frac{\tau_a}{M_{cc} H_{cc}} \\ \dot{T}_{cwo} &= \frac{[\dot{m}_{cw} H_{cw} (T_{cwi} - T_{cwo}) + \dot{m}_{sa} H_{sa} (T_{sai} - T_{sao})]}{M_{cc} H_{cc}}, \text{ if } \dot{m}_{cw} \neq 0 \\ \dot{T}_{cwo} &= \zeta \cdot (T_{cwi} - T_{cwo}), \quad \text{otherwise} \end{aligned} \quad (2)$$

The value of  $\dot{m}_{sai}$  is kept above zero to ensure minimum air flow into the zone.  $T_{cwo}$  reaches  $T_{cwi}$  when  $\dot{m}_{cw} = 0$  (with  $\zeta [s^{-1}]$ ).

### 2.1.2. Thermal Zones

To model the zones, it is assumed that the decrease in pressure at the zones and mixing box is ignored, supply air density is constant, air to the zones is mixed and temperature is distributed uniformly. Since the study is carried out for summer mode, the VAV dampers are opened as the temperature setpoint decreases. The energy equation for the  $i$ -th zone considering the above assumptions can be defined as:

$$\dot{T}_{zi} = \frac{1}{V_{zi} \rho_{sa} H_{sa}} [\dot{Q}_i + \dot{m}_{sai} H_{sa} (T_{sao} - T_{zi}) + T_{ti} A_{zi} (T_e - T_{zi})], \quad i = 1, 2. \quad (3)$$

where  $T_{ti}$  is the thermal transmittance of the zone and the capacitance effect is ignored. The definitions and numerical values of the parameters used in the mathematical modeling of the VAV system are illustrated in Tables 2 and 3 respectively.

**Table 2.** Definitions of the parameters used in the modeling of the variable air volume air conditioning system.

$M_{cc}$	cooling coil mass kg	$\dot{m}_{cw}$	mass flow rate of cold water kg/s
$\dot{m}_{sai}$	supply air flow rate kg/s	$H_{cc}$	cooling coil heat capacity J/kgK
$H_w$	cooling water heat capacity J/kgK	$H_{sa}$	supply air heat capacity J/kgK
$\rho_{sa}$	supply air density $\text{kgm}^{-3}$	$\tau_a$	coefficient for heat exchange W/K
$T_{cc}$	cooling coil temperature °C	$T_{cwo}$	cooling coil outlet water temperature °C
$T_{cwi}$	cooling coil inlet water temperature °C	$T_{sai}$	supply air inlet temperature to coil °C
$T_{sao}$	supply air outlet temperature of coil °C	$V_{zi}$	volume of $i$ -th zone $\text{m}^3$
$A_{zi}$	Area of $i$ -th zone $\text{m}^2$	$T_{ti}$	thermal transmittance of $i$ -th zone $\text{W/m}^2\text{K}$
$\dot{m}_{vi}$	$i$ -th zone air flow rate kg/s	$T_{zi}$	Temperature of $i$ -th zone °C
$\dot{Q}_i$	heat source of $i$ -th zone (internal and external) Watt	$\dot{m}_m = \dot{m}_{sa}$	flow rate of mixed air kg/s
$\dot{m}_{ra}$	flow rate of recycled air kg/s	$\dot{m}_e = \dot{m}_{sa}$	external air flow rate kg/s
$T_e$	external air temperature °C	$T_m = T_{sai}$	mixed air temperature °C
$T_{ra}$	recycled air temperature °C	$p$	percentage of recycled air %
$T_{sc} = T_{sao}$	cold air supply temperature °C		

**Table 3.** Numerical values of variable air volume system parameters on the operating point.

$M_{cc} = 2.5 \text{ kg}$	$H_{cc} = 3000 \text{ J/kgK}$
$H_w = 4200 \text{ J/kgK}$	$H_{sa} = 1000 \text{ J/kgK}$
$\rho_{sa} = 1.182 \text{ kgm}^{-3}$	$\tau_a = 24.4 \text{ W/K}$
$A_{zi} = 1218 \text{ m}^2$	$T_{ti} = 0.81 \text{ W/m}^2\text{K}$
$\dot{Q}_i = u_4, u_5 = 500, 500 \text{ Watt}$	$T_{cc} = 15 \text{ }^\circ\text{C}$
$T_e = u_6 = 27 \text{ }^\circ\text{C}$	$V_{zi} = 3690 \text{ m}^3$
$p = 0.25$	$T_{cwi} = 7 \text{ }^\circ\text{C}$

### 2.1.3. Air Mixing Box

According to the mass balance and energy equations, it follows that:

$$\begin{aligned} \dot{m}_m &= \dot{m}_{ra} + \dot{m}_e \\ T_m &= pT_{ra} + (1-p)T_e \end{aligned}$$

where

$$p := \frac{\dot{m}_{ra}}{\dot{m}_m}, \quad T_{ra} = \frac{\sum_{i=1}^2 \dot{m}_{sai} T_{zi}}{\sum_{i=1}^2 \dot{m}_{sai}} \quad (4)$$

### 2.1.4. State Space Modeling

We consider the following assumptions.

$$\begin{aligned} \alpha_1 &\equiv \frac{1}{V_{z1}\rho_{sa}}, & \alpha_2 &\equiv \frac{1}{V_{z1}\rho_{sa}H_{sa}}, & \alpha_3 &\equiv \frac{T_{t1}A_{z1}}{V_{z1}\rho_{sa}H_{sa}} \\ \beta_1 &\equiv \frac{1}{V_{z2}\rho_{sa}}, & \beta_2 &\equiv \frac{1}{V_{z2}\rho_{sa}H_{sa}}, & \beta_3 &\equiv \frac{T_{t2}A_{z2}}{V_{z2}\rho_{sa}H_{sa}}. \end{aligned} \quad (5)$$

The inputs, state variables and outputs of the VAV nonlinear model are described as:

$$\begin{aligned} u_1 &= \dot{m}_{sa1}, & u_2 &= \dot{m}_{sa2}, & u_3 &= \dot{m}_{cw}, \\ u_4 &= \dot{Q}_1, & u_5 &= \dot{Q}_2, & u_6 &= T_e, \\ x_1 &= T_{z1}, & x_2 &= T_{z2}, & x_3 &= T_{sc}, & x_4 &= T_{cwo} \\ y_1 &= x_1, & y_2 &= x_2, & y_3 &= x_3, & y_4 &= x_4 \end{aligned} \quad (6)$$

Equations (1)–(4) can be simplified as the nonlinear MIMO state space model as:

$$\begin{aligned} \dot{x}_1 &= \alpha_1 u_1 (x_3 - x_1) + \alpha_2 u_4 + \alpha_3 (u_6 - x_1), \\ \dot{x}_2 &= \beta_1 u_2 (x_3 - x_2) + \beta_2 u_5 + \beta_3 (u_6 - x_2), \\ \dot{x}_3 &= \left[ \frac{H_w u_3 (T_{cwi} - x_4)}{H_{sa} (u_1 + u_2)} + \left( p \frac{x_1 u_1 + x_2 u_2}{u_1 + u_2} + u_6 (1 - p) - x_3 \right) \right] \frac{\tau_a}{M_{cc} H_{cc}} \\ \dot{x}_4 &= \zeta \cdot (T_{cwi} - x_4), & \text{if } u_3 = 0 \\ \dot{x}_4 &= \left[ H_w u_3 (T_{cwi} - x_4) + H_{sa} (u_1 + u_2) \left( p \frac{x_1 u_1 + x_2 u_2}{u_1 + u_2} + u_6 (1 - p) - x_3 \right) \right] \\ &\times \frac{1}{M_{cc} H_{cc}}, & \text{otherwise,} \end{aligned} \quad (7)$$

we consider the following assumptions.

$$\begin{aligned} f_1 &= \alpha_2 u_4 + \alpha_3 (u_6 - x_1), \\ g_1 &= \alpha_1 (x_3 - x_1), \\ f_2 &= \beta_2 u_5 + \beta_3 (u_6 - x_2), \\ g_2 &= \beta_1 u_2 (x_3 - x_2), \\ f_3 &= \left( p \frac{x_1 u_1 + x_2 u_2}{u_1 + u_2} + u_6 (1 - p) - x_3 \right) \frac{\tau_a}{M_{cc} H_{cc}}, \\ g_3 &= \left[ \frac{H_w (T_{cwi} - x_4)}{H_{sa} (u_1 + u_2)} \right] \frac{\tau_a}{M_{cc} H_{cc}}, \end{aligned} \quad (8)$$

After simplification of Equation (7), we get:

$$\begin{aligned}\dot{x}_1 &= f_1 + g_1 \cdot u_1, \\ \dot{x}_2 &= f_2 + g_2 \cdot u_2, \\ \dot{x}_3 &= f_3 + g_3 \cdot u_3.\end{aligned}\tag{9}$$

### 3. Controller Design

#### 3.1. Sliding Mode Control

SMC is an advanced technique for nonlinear control design that possesses excellent features like robustness, easier tuning and accuracy. It uses the discontinuous signal for control and adjusts the dynamics of the system to slide along a surface known as the sliding surface, where the control can be continuously switched from one structure to another. It is also defined as the variable control structure technique because of switching. When the system is on the sliding surface, it is referred to as being in sliding mode. Figure 2 depicts the trajectory sliding on the surface and explains how SMC works. The sliding surface,  $s = 0$ , is defined in this illustration, and sliding mode begins soon after system trajectories reach the specified area. The trajectories are assumed to obey the following rules [30].

- The direction of trajectories is always towards  $s = 0$ .
- Once the sliding mode begins, the system follows  $s = cx + \dot{x} = 0$ .
- Trajectories are not allowed to leave the switching line and always belong to it.

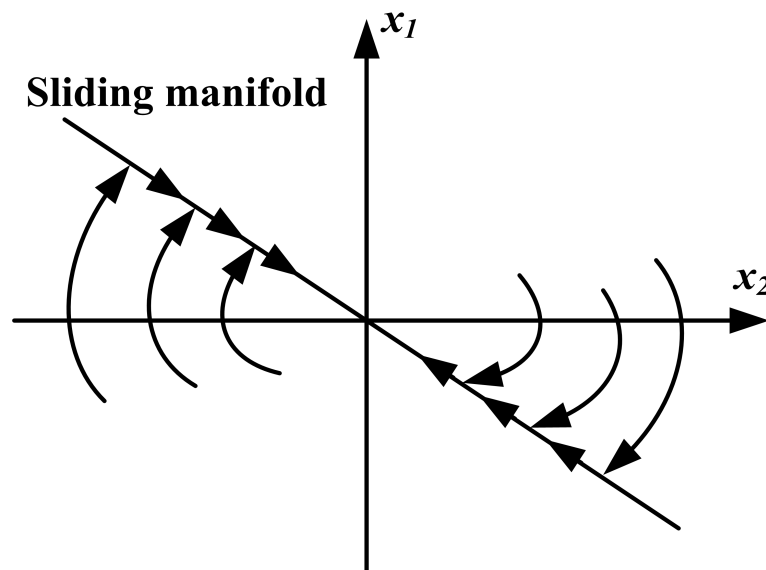


**Figure 2.** Sliding mode control (SMC) graphical representation of the sliding surface.

##### 3.1.1. Chattering Phenomena

As long as state trajectory  $x(t)$  abides the desired trajectory for  $t \geq t_o$  and  $t_o > 0$ , sliding mode is observed. It may require unlimited switching, but a practical controller has a deficiency that leads the switching to a finite number. The operating point in this situation oscillates near the sliding surface, and the phenomenon is termed as chattering. Figure 3 shows the chattering during sliding mode. Chattering is not acceptable in control design because it requires higher control actions, specially due to its involvement in higher order frequencies. If the boundary layer the near switching area is smooth, chattering can be eliminated [31].

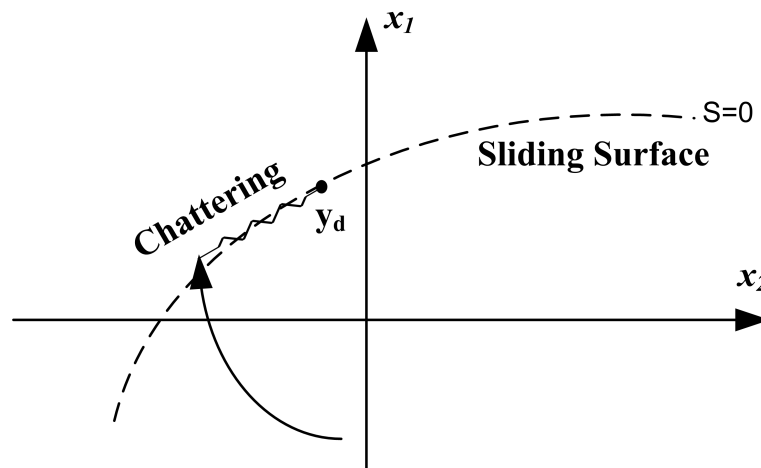


**Figure 3.** Chattering phenomena occurs during sliding mode and is practically unwanted in control design.

### 3.1.2. SMC Design

The general form of the plant can be obtained from Equation (7).

$$\ddot{x} = f(x, t) + g(t)u + d(t), \tag{10}$$

where  $f(x, t)$  and  $g(t)$  are known and  $d(t)$  is unknown disturbance,  $|d(t)| \leq D$ . The function for sliding mode can be designed as:

$$s(t) = he(t) + \dot{e}(t), \tag{11}$$

In (11),  $h > 0$  is designed to satisfy the Hurwitz criteria, and the tracking error and its respective derivative are defined as:

$$\begin{aligned} e &= x_d - x_1, \\ \dot{e} &= \dot{x}_d - \dot{x}_1, \end{aligned} \tag{12}$$

where  $x_d$  is an ideal signal.

$$\begin{aligned} \dot{s} &= h\dot{e} + \ddot{e} \\ &= h(\dot{x}_d - \dot{x}_1) + (\ddot{x}_d - \ddot{x}) \\ &= h(\dot{x}_d - \dot{x}_1) + (\ddot{x}_d - f - g.u - d). \end{aligned} \tag{13}$$

By using the exponential reaching law,

$$\dot{s} = -\epsilon \operatorname{sgn} s - ps, \quad \epsilon, p > 0. \tag{14}$$

The solution of the exponential term  $\dot{s} = -ks$  is,  $s = s(0)e^{-kt}$ . With the larger  $s$  value, the state will approach faster towards the switching manifold. Form Equations (13) and (14),

$$h(\dot{x}_d - \dot{x}_1) + (\ddot{x}_d - f - g.u - d) = -\epsilon \operatorname{sgn} s - ps. \tag{15}$$

The control law can be represented as:

$$u(t) = \frac{1}{g}(\epsilon \operatorname{sgn} s) + ps + h(\dot{x}_d - \dot{x}_1 + \ddot{x}_d - f - d), \tag{16}$$

all the values are known except  $d$ . Redesigning the control law, we get:

$$u(t) = \frac{1}{g}(\epsilon \operatorname{sgn} s) + ps + h(\dot{x}_d - \dot{x}_1 + \ddot{x}_d - f - D\operatorname{sgn}s), \tag{17}$$

rearranging Equations (13) and (17), we have:

$$\dot{s} = -\epsilon \operatorname{sgn} s - ps - D \operatorname{sgn} s - d. \quad (18)$$

It follows that:

$$\begin{aligned} s\dot{s} &= s(-\epsilon \operatorname{sgn} s - ps - D \operatorname{sgn} s - d) \\ &= -ps^2 - \epsilon \log |s| - D \log |s| - ds. \end{aligned} \quad (19)$$

For stability analysis, the Lyapunov function

$$V = \frac{1}{2}s^2$$

is adopted.

$$\dot{V} = s\dot{s}(t) = -ps^2 - \epsilon \log |s| - D \log |s| - ds \leq -2pV. \quad (20)$$

After further simplification [31],

$$V(t) \leq e^{-2pt}V(0). \quad (21)$$

Eventually, with a positive  $p$  value, the sliding mode function converges to zero exponentially. From Equation (7), we have three equations for  $\dot{x}_1$ ,  $\dot{x}_2$  and  $\dot{x}_3$ . By adopting the same procedure of control design, the three control laws can be obtained as follows.

$$\begin{aligned} u_1(t) &= \frac{1}{g_1}(\epsilon \operatorname{sgn} s) + ps + h(\dot{x}_i - \dot{x}_1 + \ddot{x}_d - f_1 - D \operatorname{sgn} s), \\ u_2(t) &= \frac{1}{g_2}(\epsilon \operatorname{sgn} s) + ps + h(\dot{x}_i - \dot{x}_1 + \ddot{x}_d - f_2 - D \operatorname{sgn} s), \\ u_3(t) &= \frac{1}{g_3}(\epsilon \operatorname{sgn} s) + ps + h(\dot{x}_i - \dot{x}_1 + \ddot{x}_d - f_3 - D \operatorname{sgn} s). \end{aligned} \quad (22)$$

The values of  $u_4$ ,  $u_5$  and  $u_6$  are presented in Table 3.

### 3.2. PID

PID controllers are the most famous among those used in industrial applications. They consist of three terms, namely proportional (P), integral (I) and derivative (D). They are mostly used to control pressure, flow, temperature, level, vibration, etc. The basic working of PID is presented in Figure 4 [32].

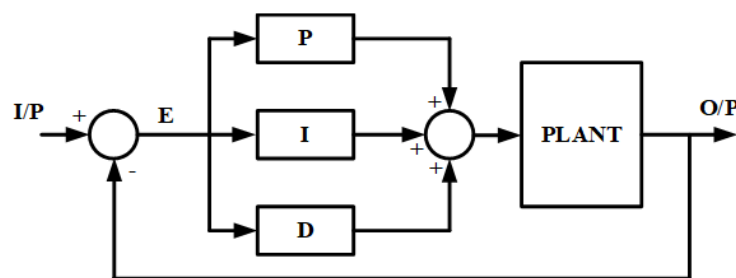


Figure 4. Basic block diagram of a proportional integral derivative (PID) controller.

$$u(t) = k_p \cdot e(t) + k_i \cdot \int e(t)dt + k_d \cdot \frac{de(t)}{dt} \quad (23)$$

Tuning is an important part in designing PID controllers. Therefore, the Ziegler–Nichols method for tuning is adopted in this study. This method involves changing the PID into P by setting values of

$K_i = \infty$  and  $K_d = 0$ . Firstly, set  $K_p = 0$ ; secondly, in program mode, close the controller loop. Keep increasing the value of  $K_p$  unless it shows less oscillations. Finally, obtain a precise period  $\alpha$  of the stable oscillations. The controller parameters are selected by utilizing the values given in Table 4.

**Table 4.** Conditions for the controller parameters in the Ziegler–Nichols’ closed loop technique.

Control Function	$K_p$	$K_i$	$K_d$
P (Proportional)	$0.5 K_\alpha$	$\infty$	0
PI (Proportional integral)	$0.45 K_\alpha$	$\frac{\alpha}{2}$	0
PID (Proportional integral derivative)	$0.6 K_\alpha$	$\frac{\alpha}{2}$	$\frac{\alpha}{8} = \frac{P_i}{4}$

#### 4. Results

The tracking objective for both strategies, PID and SMC, is studied in this section. For the temperature setpoint of Zone 1 and Zone 2, two practical waveforms including sinusoidal and the combination of steps were considered; presented in Figure 5. Figure 5a,c is the temperature setpoint for Zone 1 and Figure 5b,d the temperature setpoint for Zone 2. The setpoints were assumed according to weather conditions in summer having a higher outside temperature. The designed strategies were applicable for all types of weather conditions. Figure 6 shows the tracking result by the PID and SMC of the Zone 1 sinusoidal temperature setpoint. In the magnified figure, it is obvious that the PID shows more overshoot in the beginning and also does not completely track the setpoint; whereas, SMC is tracking the setpoint effectively with negligible overshoot and the steady state. The performance of both controllers for the Zone 2 sinusoidal setpoint is presented in Figure 7. SMC shows a robust behavior while tracking the target, whereas PID lags in accurate tracking of the sinusoidal reference.

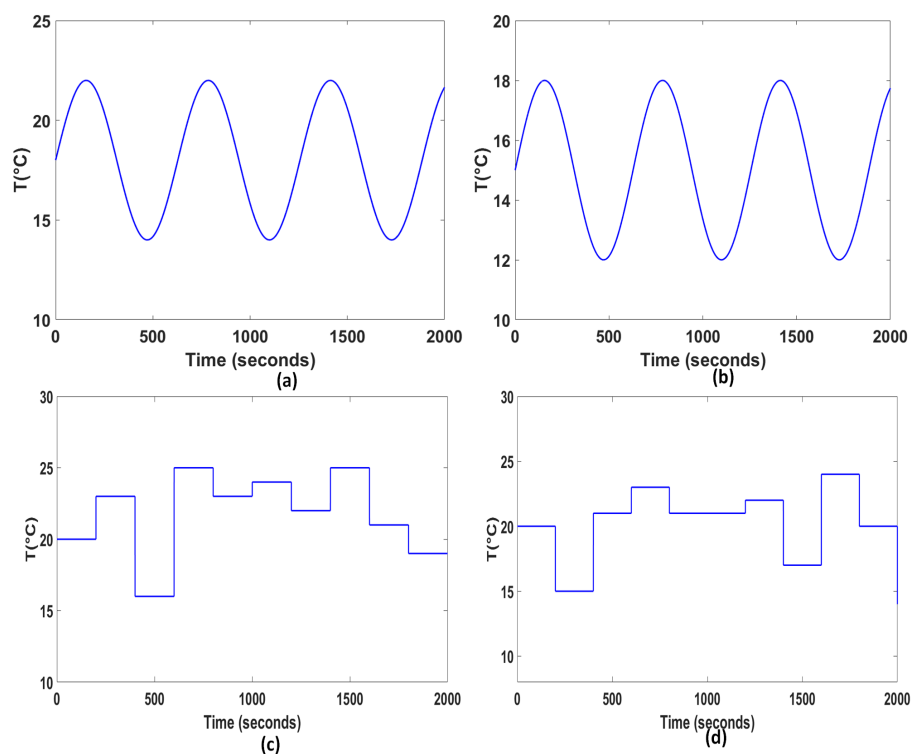


**Figure 5.** Setpoint temperature range for (a) Zone 1 sine wave reference, (b) Zone 2 sine wave reference, (c) Zone 1 reference signal having the sequence of steps and (d) Zone 2 reference signal having the sequence of steps.

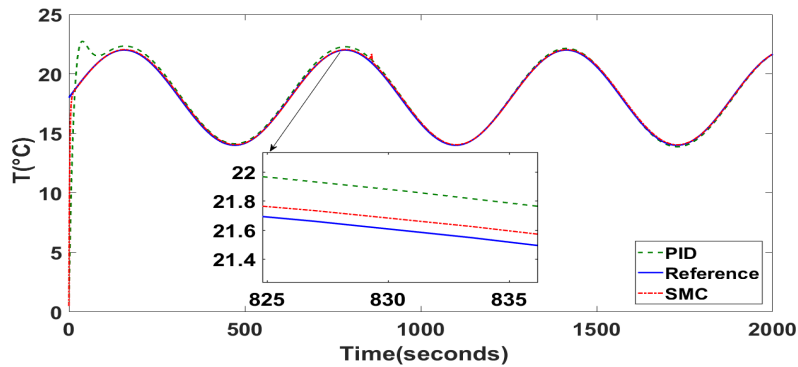


Figure 6. Tracking result of the PID and SMC for Zone 1 sine wave reference.

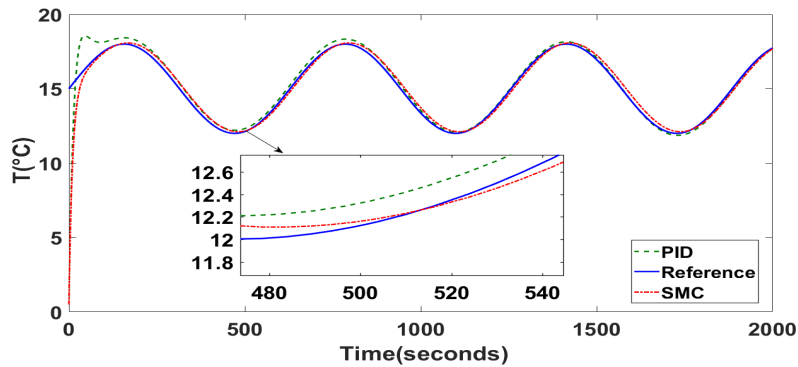


Figure 7. Tracking result of PID and SMC for Zone 2 sine wave reference.

Figure 8 shows the combination of steps setpoint for Zone 1 temperature. Here, PID shows more overshoot at all step changes in the temperature setpoints, while SMC shows less overshoot in the beginning. Furthermore, it is clear from the zoomed part that SMC shows a negligible settling time. For Zone 2, different magnitudes of the combinations of steps were applied, as shown in Figure 9. Again, SMC showed a better tracking result, while clearly, PID gave the maximum overshoot and settling time. The reason behind the inefficiency of the PID controller is because these controllers are not efficient for nonlinear systems with uncertainties, as compared to SMC; also, HVAC systems are highly nonlinear and influenced by uncertainties because of parametric variations and external disturbances. Furthermore, PID does not handle abrupt changes in the setpoint, and it is also not a robust controller; therefore, it shows more overshoot and the steady state for all of the setpoints. Since the temperature in the duct was constant and the temperature of supply air was controlled by the cooling water flow rate in the coil, the change in temperature of the supply air and cold water by PID and SMC was also analyzed.

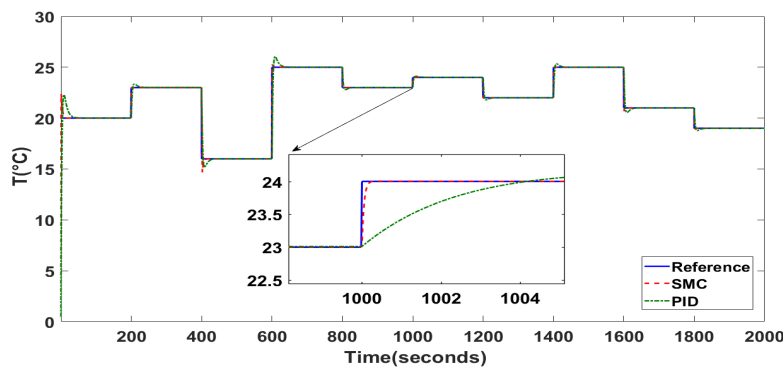
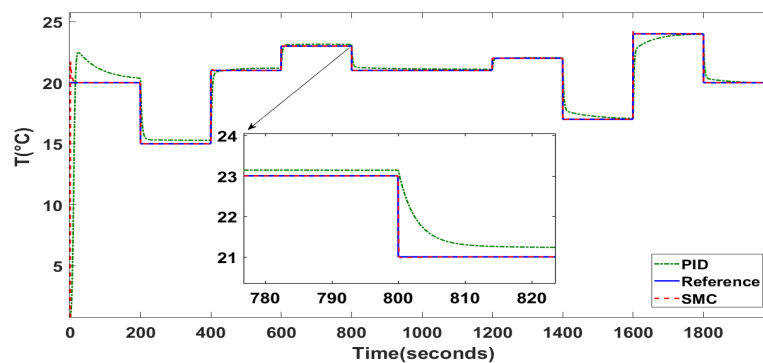
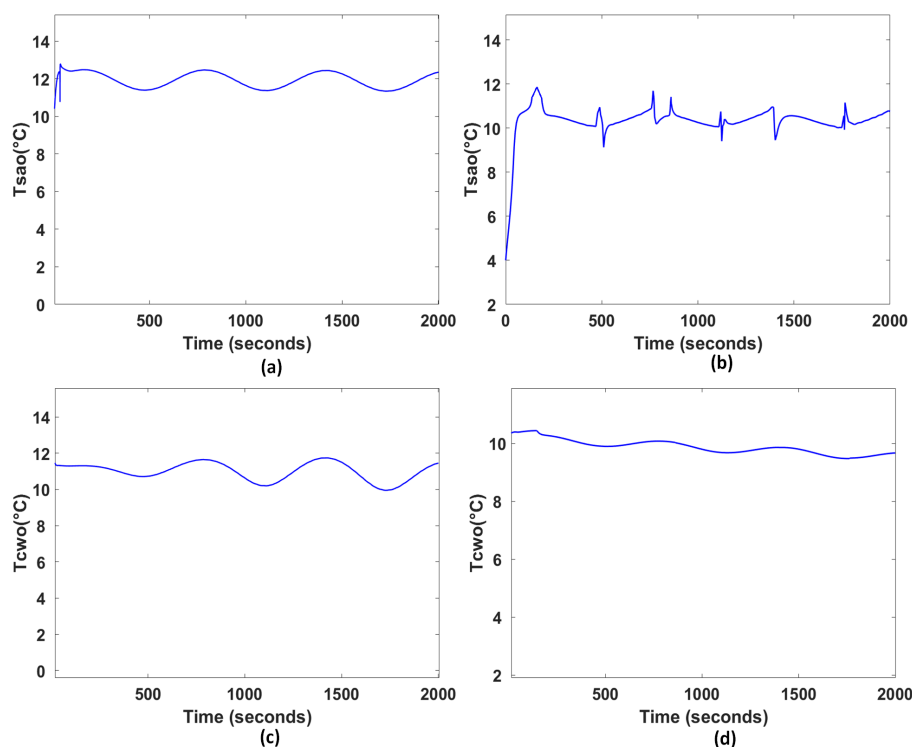


Figure 8. Tracking result of PID and SMC for the Zone 1 combination of steps reference.



**Figure 9.** Tracking result of PID and SMC for the Zone 2 combination of steps reference.

Figure 10a shows  $T_{sao}$  by the PID controller for the sinusoidal reference of Zone 1 and Zone 2, and the same  $T_{sao}$  supplied by SMC is represented in Figure 10b. SMC showed continuous variations and a smooth supply of the air because temperature setpoint was varying for both zones continuously, whereas PID shows lower variations and cannot track the setpoint effectively. The output water temperature from the cooling coil was also analyzed to check its performance. The inlet water temperature  $T_{cwi}$  was set to 7 °C, since any lower water temperature than this could cause freezing problems in the coil. Output water temperature  $T_{cwo}$  from the cooling coil by PID is presented in Figure 10c, and that for SMC is presented in Figure 10d, which shows the normal operation of the coil.



**Figure 10.** Output temperature results of, (a) supply air ( $T_{sao}$ ) from the PID controller for the sine wave reference of Zone 1 and Zone 2, (b) supply air ( $T_{sao}$ ) from SMC for the sine wave reference of Zone 1 and Zone 2, (c) cooling coil water outlet temperature ( $T_{cwo}$ ) from the PID controller for the sine wave reference of Zone 1 and Zone 2 and (d) cooling coil water outlet temperature ( $T_{cwo}$ ) from SMC for the sine wave reference of Zone 1 and Zone 2.

Similarly, the air supply  $T_{sao}$  for the combination of steps temperature setpoint to Zone 1 and Zone 2 by PID and SMC is presented in Figure 11a,b respectively. Since variations were continuously

occurring in the setpoint, SMC handled these variations more effectively than PID while maintaining the required amount of cold supply air to both zones. PID again lagged in the required amount of air supply. Water output  $T_{cwo}$  from the cooling coil by PID and SMC for the combination of steps reference is presented in Figure 11c,d. Again, the temperature of the outlet water showed the normal operations of the system.

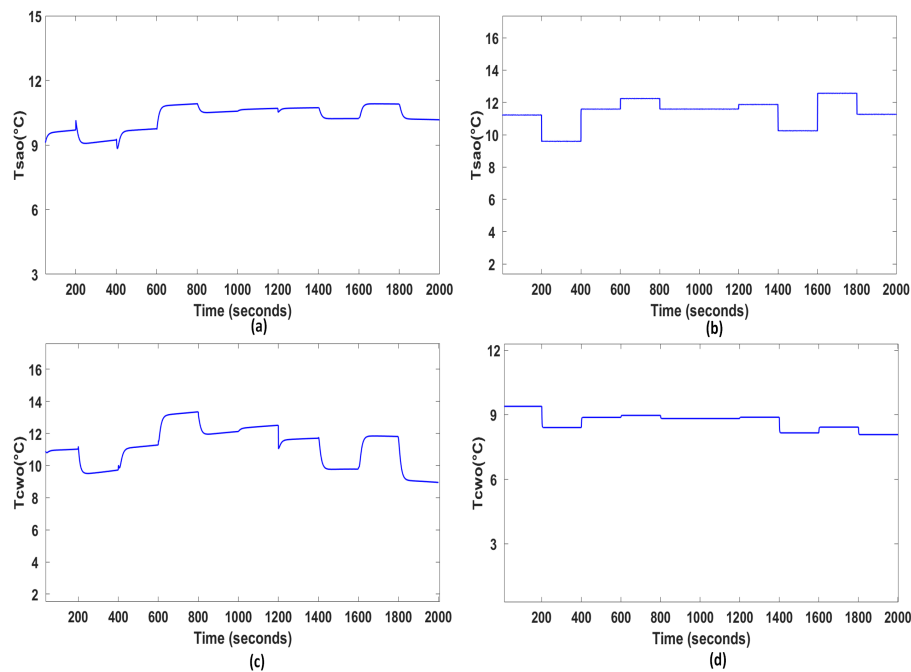


**Figure 11.** Output temperature results of, (a) supply air (Tsao) from the PID controller for the combination of steps reference of Zone 1 and Zone 2, (b) supply air (Tsao) from SMC for the combination of steps reference of Zone 1 and Zone 2, (c) cooling coil water outlet temperature (Tcwo) from the PID controller for the combination of steps reference of Zone 1 and Zone 2 and (d) cooling coil water outlet temperature (Tcwo) from SMC for the combination of steps reference of Zone 1 and Zone 2.

To analyze controller performance by SMC and PID for sinusoidal reference temperature the setpoint and combinations of steps, we have four cases for three manipulated variables. Figure 12a shows  $u_1$  (flow rate of cold supply air to Zone 1), Figure 12b shows  $u_2$  (flow rate of cold supply air to Zone 2) and  $u_3$  (flow rate of cold water) is shown in Figure 12c for the PID controller having a sinusoidal reference.

The control effort of SMC on the same reference in Figure 13a shows  $u_1$ ; Figure 13b shows  $u_2$ ; and Figure 13c shows  $u_3$ . By comparing the control effort for PID and SMC, it is obvious that SMC was responding according to the abrupt variations in setpoints, whereas PID was not responding according to the variations in setpoint temperature, and this is the reason that PID was showing more overshoot and steady state error for all of the setpoints.

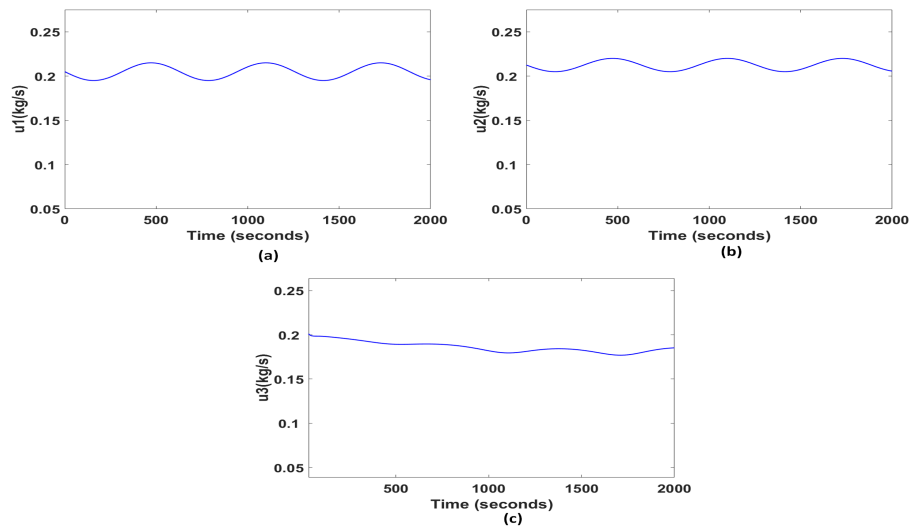


**Figure 12.** Control efforts: (a)  $u_1$ , (b)  $u_2$  and (c)  $u_3$  by the PID controller for the sine wave reference (Zone 1 and Zone 2).

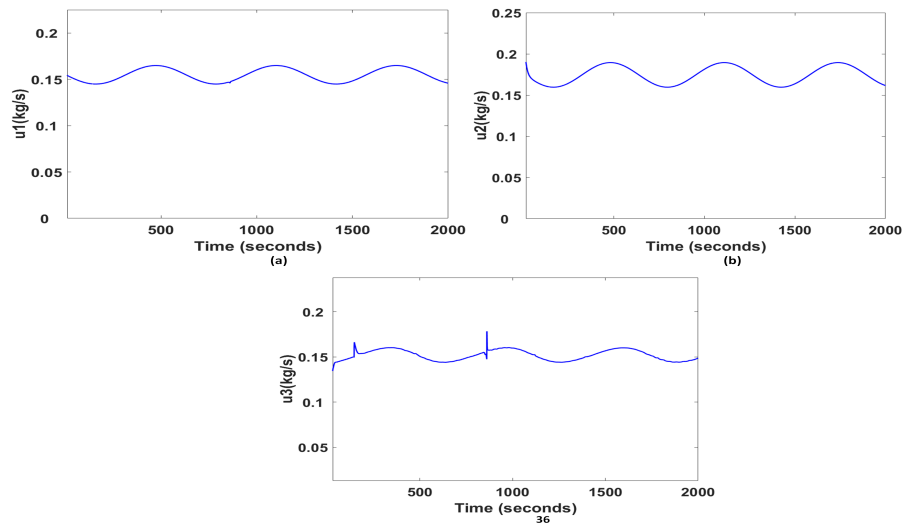


**Figure 13.** Control efforts: (a)  $u_1$ , (b)  $u_2$  and (c)  $u_3$  by SMC for the sine wave reference (Zone 1 and Zone 2).

The combination of steps reference for the PID control effort is presented in Figure 14a for  $u_1$ , in Figure 14b for  $u_2$  and  $u_3$  in Figure 14c.

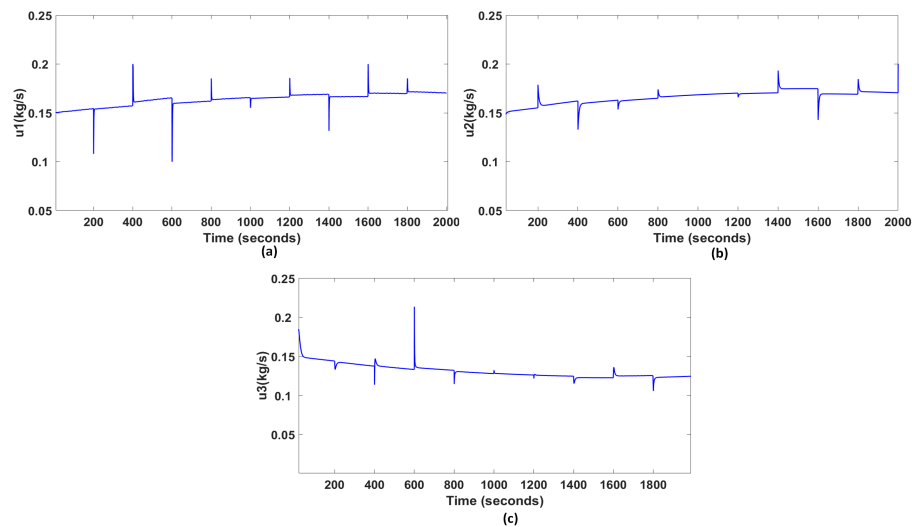


**Figure 14.** Control efforts: (a)  $u_1$ , (b)  $u_2$  and (c)  $u_3$  by the PID controller for the combination of steps reference (Zone 1 and Zone 2).

The respective SMC control effort is presented in Figure 15a for  $u_1$ , in Figure 15b for  $u_2$  and  $u_3$  in Figure 15c. The air supply to zones was maintained by dampers, and from the results, it is clear that flow rate variations matched with the variations in the temperature setpoint of the respective zone. Once again, SMC outperformed the PID in the control action.

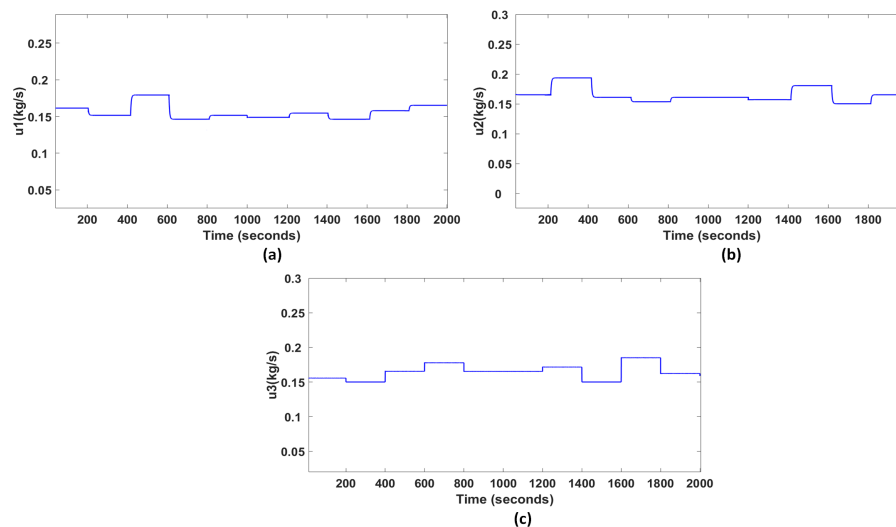


**Figure 15.** Control efforts: (a)  $u_1$ , (b)  $u_2$  and (c)  $u_3$  by SMC for the combination of steps reference (Zone 1 and Zone 2).

The performance index is a common criteria to measure the performance of the system and is adopted to focus on essential system particulars. The system is considered as a perfect control system, when the index reaches the minimum values on selected settings. Four types of performance indices are used to analyze the controllers' performance.

- Integral time absolute error (ITAE).

$$ITAE = \int_0^T t|e(t)|dt$$

- Integral of absolute error (IAE).

$$IAE = \int_0^T |e(t)| dt$$

- Integral of squared error (ISE).

$$ISE = \int_0^T e^2(t) dt$$

- Integral time squared error (ITSE).

$$ITSE = \int_0^T te^2(t) dt$$

Table 5 shows the numerical values calculated by the performance index of SMC and PID controllers. Values of  $u_1$ ,  $u_2$  and  $u_3$  for the combination of steps and sine wave reference show that SMC had the minimum values for all four types of errors as compared to PID.

**Table 5.** Performance indices values of  $u_1$ ,  $u_2$  and  $u_3$  for both SMC and the PID controller. ITAE, integral time absolute error; IAE, integral of absolute error; ISE, integral of squared error; ITSE, integral time squared error.

Controller	Combination of Steps				Sine Wave			
	ITAE	IAE	ISE	ITSE	ITAE	IAE	ISE	ITSE
<b>PID</b>								
$u_1$	$3.106 \times 10^6$	2902	5520	$6.002 \times 10^6$	$8.001 \times 10^5$	742	392.1	$4.165 \times 10^5$
$u_2$	$1.125 \times 10^5$	352.5	3010	$2.137 \times 10^5$	$1.91 \times 10^5$	175.8	236.7	$1.402 \times 10^4$
$u_3$	9010	9.101	0.610	311.6	$2.575 \times 10^7$	$2.534 \times 10^4$	$3.875 \times 10^5$	$4.054 \times 10^8$
<b>SMC</b>								
$u_1$	$1.365 \times 10^4$	3000	101.1	$2.10 \times 10^4$	$1.224 \times 10^5$	166.1	321.8	$1.40 \times 10^4$
$u_2$	$1.00 \times 10^4$	22.10	95.19	9360	$1.492 \times 10^5$	158.4	146	8956
$u_3$	$2.015 \times 10^6$	2020	2410	2012	$1.577 \times 10^5$	155.7	12.35	$2.328 \times 10^6$

## 5. Conclusions

In this paper, a nonlinear minimum phase VAV multiple zone model is considered, and two control strategies including PID and SMC are designed. First, the mathematical model of multizone VAV is established in the form of nonlinear state space. Then, two control techniques are compared from different perspectives including minimum control effort and reduced energy consumption level in terms of overshoot and settling time. In addition, four performance indices namely integral time absolute error (ITAE), integral time squared error (ITSE), integral of squared error (ISE) and integral of absolute error (IAE) are also evaluated for both controllers. The individual zone temperature is controlled by adjusting damper position according to zone temperature setpoint. The cold air supply temperature and cooling coil water outlet temperature are analyzed to ensure normal operation of the system. Two realistic command temperature setpoints including the combination of steps and sinusoidal wave are chosen as a setpoint temperature to evince the robust tracking by controllers. After extensive simulations in MATLAB, it is concluded that the PID controller has unsatisfactory behavior compared to SMC. The SMC shows robust performance in terms of less overshoot, settling time and lesser performance index values during tracking of the setpoint, which makes SMC more energy efficient. The following conclusions are drawn from the results obtained:

- Both controllers track the desired commands, but SMC outperforms PID in all aspects of control actions.
- Since the zones temperatures are dynamically coupled with each other, this effect is decoupled by the integral action of PID and high gain inherent to SMC.

- Performance index values including all four types of errors are minimum for SMC as compared to PID.
- SMC ensures robustness by effectively tracking the setpoints in the existence of uncertainties with less overshoot and settling time, which makes SMC more energy efficient.

**Author Contributions:** Conceptualization, A.S.; Methodology, D.H.; Software, A.S.; Validation, A.S. and U.F.; Formal Analysis, T.H.; Investigation, A.S.; Resources, T.H.; Data Curation, U.F.; Writing-Original Draft Preparation, A.S.; Writing-Review and Editing, A.S.; Visualization, U.F.; Supervision, D.H.; Project Administration, D.H.; Funding Acquisition, T.H.

**Funding:** The work was partially supported by the National Natural Science Foundation of China under Grants 61773323, 61433011, 61603316, 61733015 and the Fundamental Research Funds for the Central Universities 2682018CX15.

**Conflicts of Interest:** The authors declare no conflict of interest.

## Nomenclature

AHU	Air handling unit
ANN	Artificial neural networks
ARX	Auto-regressive exogenous
DBN	Diagnostic Bayesian network
DFL	Direct feedback linear
EWMA	Exponentially weighted moving average
HMS	Health monitoring system
HVAC	Heating ventilating and air conditioning
IAQ	Indoor air quality
MIMO	Multiple input multiple output
MPC	Model predictive control
PID	Proportional integral derivative
RGA	Relative gain array
SISO	Single input single output
SMC	Sliding mode controller
SVM	Support vector machine
VAV	Variable air volume
VRF	Variable refrigerant flow

## References

1. Chua, K.J.; Chou, S.K.; Yang, W.M.; Yan, J. Achieving better energy-efficient air conditioning—A review of technologies and strategies. *Appl. Energy* **2013**, *104*, 87–104. [[CrossRef](#)]
2. Okochi, G.S.; Yao, Y. A review of recent developments and technological advancements of variable-air-volume (VAV) air-conditioning systems. *Renew. Sustain. Energy Rev.* **2016**, *59*, 784–817. [[CrossRef](#)]
3. Lee, S.; Kim, H.; Dong, H.; Jeong, J. Energy saving assessment of a desiccant-enhanced evaporative cooling system in variable air volume applications. *Appl. Therm. Eng.* **2017**, *117*, 94–108. [[CrossRef](#)]
4. Moradi, H.; Setayesh, H.; Alasty, A. PID-Fuzzy control of air handling units in the presence of uncertainty. *Int. J. Therm. Sci.* **2016**, *109*, 123–135. [[CrossRef](#)]
5. Zhai, Z.; Johnson, S.N. Full-Scale Laboratory Test on Energy Dependence on Pressure Drops in HVAC Systems. *Procedia Eng.* **2017**, *205*, 2133–2140. [[CrossRef](#)]
6. Wang, G.; Song, L. Air handling unit supply air temperature optimal control during economizer cycles. *Energy Build.* **2012**, *49*, 310–316. [[CrossRef](#)]
7. Shah, A.; Huang, D.; Chen, Y.; Kang, X.; Qin, N. Robust Sliding Mode Control of Air Handling Unit for Energy Efficiency Enhancement. *Energies* **2017**, *10*, 1815. [[CrossRef](#)]
8. Yao, Y.; Yang, K.; Huang, M.; Wang, L. A state-space model for dynamic response of indoor air temperature and humidity. *Build. Environ.* **2013**, *64*, 26–37. [[CrossRef](#)]
9. Zhu, Y.; Jin, X.; Du, Z.; Fang, X. Online optimal control of variable refrigerant flow and variable air volume combined air conditioning system for energy saving. *Appl. Therm. Eng.* **2015**, *80*, 87–96. [[CrossRef](#)]

10. Attaran, S.M.; Yusof, R. Enhancement of control's parameter of decoupled hvac system via adaptive controller through the system identification tool box. *J. Teknol.* **2015**, *76*, 1. [[CrossRef](#)]
11. Shi, Z.; Li, X.; Hu, S. Direct Feedback Linearization Based Control in Variable Air Volume air-conditioning System. *Phys. Procedia* **2012**, *24*, 1248–1254. [[CrossRef](#)]
12. Pang, X.; Piette, M.A.; Zhou, N. Characterizing variations in variable air volume system controls. *Energy Build.* **2017**, *135*, 166–175. [[CrossRef](#)]
13. Xu, X.; Zhong, Z.; Deng, S.; Zhang, X. A review on temperature and humidity control methods focusing on air-conditioning equipment and control algorithms applied in small-to-medium-sized buildings. *Energy Build.* **2018**, *162*, 163–176. [[CrossRef](#)]
14. Tukur, A.; Hallinan, K. Statistically informed static pressure control in multiple-zone VAV systems. *Energy Build.* **2017**, *135*, 244–252. [[CrossRef](#)]
15. Kang, S.; Kim, H.; Cho, Y. A study on the control method of single duct VAV terminal unit through the determination of proper minimum air flow. *Energy Build.* **2014**, *69*, 464–472. [[CrossRef](#)]
16. Kang, C.; Park, J.; Park, M.; Baek, J. Novel Modeling and Control Strategies for a HVAC System Including Carbon Dioxide Control. *Energies* **2014**, *7*, 3599–3617. [[CrossRef](#)]
17. Kaam, S.; Raftery, P.; Cheng, H.; Paliaga, G. Time-averaged ventilation for optimized control of variable-air-volume systems. *Energy Build.* **2017**, *139*, 465–475. [[CrossRef](#)]
18. Chuang, H.; Chi, J.; Chang, K.; Lee, C. Study on a fan coil unit and chiller by an intelligent control method with a stepless variable speed driving technology. *Build. Environ.* **2018**, *132*, 137–146. [[CrossRef](#)]
19. Yang, X.; Jin, X.; Du, Z.; Fan, B.; Chai, X. Evaluation of four control strategies for building VAV air-conditioning systems. *Energy Build.* **2011**, *43*, 412–422. [[CrossRef](#)]
20. Li, X.; Zhao, T.; Zhang, J.; Chen, T. Prediction control for indoor temperature time-delay using Elman neural network in variable air volume system. *Energy Build.* **2017**, *154*, 545–552. [[CrossRef](#)]
21. Cutillas, C.G.; Ramírez, J.R.; Miralles, M.L. Optimum Design and Operation of an HVAC Cooling Tower for Energy and Water Conservation. *Energies* **2017**, *10*, 299. [[CrossRef](#)]
22. Serale, G.; Fiorentini, M.; Capozzoli, A.; Bernardini, D.; Bemporad, A. Model Predictive Control (MPC) for Enhancing Building and HVAC System Energy Efficiency: Problem Formulation, Applications and Opportunities. *Energies* **2018**, *11*, 631. [[CrossRef](#)]
23. Schirrer, A.; Brandstetter, M.; Leobner, I.; Hauer, S.; Koze, M. Nonlinear model predictive control for a heating and cooling system of a low-energy office building. *Energy Build.* **2016**, *125*, 26–98. [[CrossRef](#)]
24. Huang, G. Model predictive control of VAV zone thermal systems concerning bi-linearity and gain nonlinearity. *Control Eng. Pract.* **2011**, *19*, 700–710. [[CrossRef](#)]
25. Liang, W.; Quinte, R.; Jia, X.; Sun, J. MPC control for improving energy efficiency of a building air handler for multi-zone VAVs. *Build. Environ.* **2015**, *92*, 256–268. [[CrossRef](#)]
26. Alamin, Y.; Castilla, M.; Álvarez, J.; Ruano, A. An Economic Model-Based Predictive Control to Manage the Users' Thermal Comfort in a Building. *Energies* **2017**, *10*, 321. [[CrossRef](#)]
27. Allen, W.H.; Rubaai, A.; Chawla, R. Fuzzy Neural Network-Based Health Monitoring for HVAC System Variable-Air-Volume Unit. *IEEE Trans. Ind. Appl.* **2015**, *52*, 2513–2524. [[CrossRef](#)]
28. Wu, Z.; Jia, Qi.; Guan, X. Optimal Control of Multiroom HVAC System: An Event-Based Approach. *IEEE Trans. Control Syst. Technol.* **2016**, *24*, 662–669. [[CrossRef](#)]
29. Behrooz, F.; Mariun, N.; Marhaban, M.; Radzi, M.M.; Ramli, A. Review of Control Techniques for HVAC Systems—Nonlinearity Approaches Based on Fuzzy Cognitive Maps. *Energies* **2018**, *11*, 495. [[CrossRef](#)]
30. Khalil, H.K. *Nonlinear Systems*, 3rd ed.; Pearson: London, UK, 2011; ISBN 978-0130673893.
31. Liu, J. *Sliding Mode Control Using MATLAB*, 1st ed.; Academic Press: Cambridge, MA, USA, 2017; ISBN 978-0128025758.
32. Åström, K.J.; Hägglund, T. *Advanced PID Control*; International Society of Automation, Inc.: Eindhoven, The Netherlands, 2005; ISBN 978-1556179426.

